

Fig. 2. Visual Lifting Bipedal Walking Strategy

the singularity. On the other hand, human looks like using intentionally the singular configuration to walk despite the above difficulties, making human's walking posture upright. On this view point, the strategy of utilizing $J(q)^T$ may have wider potential than $J(q)^{-1}$ to help the robot realize human-like walking.

In this paper we propose Visual Lifting Stable Walking scheme based on a visual servoing concept, utilizing 1-step GA real-time pose tracking method [8], [9]. We use dual cameras as the humanoid's eyes, to observe a static object that is set in the right front to measure the robot's head pose based on the object through visual pose estimation ([10]-[12]) during walking or just standing (Fig.1). $J(q)^T$ is used in our research to project stabilizing force and torque that is calculated by visual measurement onto each joint, exemplifying the possibility for stable walking by using a dynamical model including various walking gait patterns. The decreased robot head may lead to falling to the ground, therefore we use the pose deviation from a desired head pose (height and orientation) to deduce a pulling up force of head by using joint torques, which are calculated through the Jacobian-transpose and lifting force desired by the detected head pose sinking deviation. We will introduce this strategy in the following section.

II. VISUAL LIFTING BIPEDAL WALKING STRATEGY

Here, we use two cameras that are set as the humanoid's eyes to measure the pose of a object being set stationarily in the right front, to perform vision-feedback control for improving humanoid's standing/walking stability.

We use a model-based matching method to measure the pose of a target object denoted by ψ based on a moving coordinates Σ_H , which represents the robot's head. we use a "1-step GA" method to solve the model matching optimization problem to realize online visual pose estimation [10].

The desired relative pose of Σ_M (target object coordinate) and Σ_H is predefined by Homogeneous Transformation as

${}^{Hd}\mathbf{T}_M(t)$. The difference of the desired head pose Σ_{Hd} and the current pose Σ_H is denoted as ${}^H\mathbf{T}_{Hd}$, it can be described by

$${}^H\mathbf{T}_{Hd}(\delta\psi(t)) = {}^H\mathbf{T}_M(\hat{\psi}(t)) {}^{Hd}\mathbf{T}_M^{-1}(\psi_d(t)), \quad (1)$$

where ${}^H\mathbf{T}_M(t)$ is calculated by $\hat{\psi}(t)$ that is measured by online visual pose estimation method.

Here, the force exerted on the head to minimize the difference of the desired head pose and the current pose ${}^H\mathbf{T}_{Hd}$ —the pose deviation of the robot's head caused by gravity force and walking dynamical influences—is considered to be directly proportional to $\delta\psi(t)$, so we have

$$\mathbf{f}_v = \mathbf{k}_v \delta\psi(t). \quad (2)$$

The above Visual Lifting Bipedal Walking strategy is depicted in Fig. 2.

The joint torque and force τ_v to be input to realize \mathbf{f}_v at the head has following relation [16]

$$\tau_v = \mathbf{J}_v^T \mathbf{f}_v, \quad (3)$$

where \mathbf{J}_v is a Jacobian matrix of the head pose against joint angles. We use τ_v to control the humanoid robot keeping stable standing/walking, by compensating the falling down action caused by gravity or dangerous slipping motion happened unpredictably etc. by using the visual feedback information. Simulation will be conducted to confirm the effectiveness of our proposed control method, and the result will be shown later in this paper.

III. BIPEDAL WALKING MODEL

A. Dynamics of Walking

The humanoid robot consists of a body, legs, and eyes (Fig.1), which has 10 degrees of freedom. Each link has mass m , length l , radius of link r , and inertia moment I , and each joint has viscous friction D .

Here as a fundamental research we set conditions that the angles of body and legs rotate around x direction of Σ_W . When the robot walks forward, the robot is getting closer to the static target object, so it is necessary to change the pose

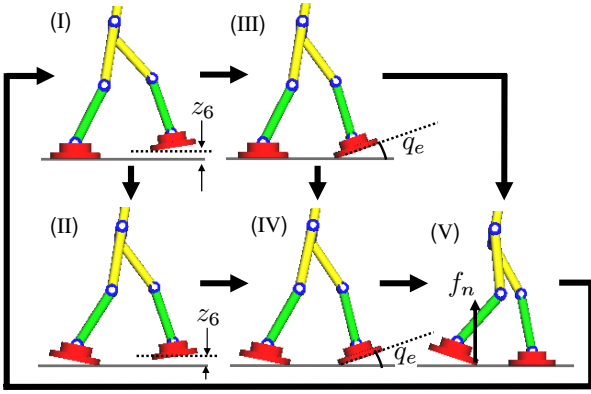


Fig. 3. Style transition diagram for bipedal walking

of the cameras to keep the object always in both views of the left and right cameras. Therefore, there are angles to rotate cameras around z direction of Σ_W to change eyes' gazing direction.

The equations of motion that includes point-constraint condition including contacting friction is written as

$$M(\mathbf{q})\ddot{\mathbf{q}} + \mathbf{h}(\mathbf{q}, \dot{\mathbf{q}}) + \mathbf{g}(\mathbf{q}) + \mathbf{D}\dot{\mathbf{q}} = \boldsymbol{\tau} + \left\{ \left(\frac{\partial C}{\partial \mathbf{q}^T} \right)^T / \left\| \frac{\partial C}{\partial \mathbf{r}^T} \right\| \right\} f_n - \left(\frac{\partial \mathbf{r}}{\partial \mathbf{q}^T} \right)^T \frac{\dot{\mathbf{r}}}{\|\dot{\mathbf{r}}\|} f_t. \quad (4)$$

M is inertia matrix, \mathbf{h} and \mathbf{g} indicate Coriolis force, centrifugal force and gravity, \mathbf{D} is matrix that indicates coefficients of joints' viscous friction. \mathbf{q} is joint angle and $\boldsymbol{\tau}$ is input torque. Then, f_n is constraint force and f_t is friction. Here, we set two reasonable assumptions: (i) f_n and f_t are orthogonal. (ii) $f_t = K f_n$ (K is proportional constant).

In addition, C is defined as point-constraint condition $C(\mathbf{r}(\mathbf{q})) = 0$, where $\mathbf{r}(\mathbf{q})$ is lifting foot's pose vector. This constraint condition happens to appear when the lifting foot's z -position in Σ_W being zero or below zero, otherwise the second and third terms of right-hand side of Eq.(4) disappear. The constraint condition concerning $\ddot{\mathbf{q}}$ given by differentiating $C(\mathbf{r}(\mathbf{q})) = 0$ by two times is written as

$$\dot{\mathbf{q}}^T \left\{ \frac{\partial}{\partial \mathbf{q}} \left(\frac{\partial C}{\partial \mathbf{q}^T} \right) \right\} \dot{\mathbf{q}} + \left(\frac{\partial C}{\partial \mathbf{q}^T} \right) \ddot{\mathbf{q}} = 0. \quad (5)$$

Abbreviating the coefficient vectors of f_n and f_t in Eq.(4) by \mathbf{j}_c^T and \mathbf{j}_t^T , Eq.(4) and Eq.(5) can be combined as follows.

$$\begin{bmatrix} M(\mathbf{q}) & -(\mathbf{j}_c^T - \mathbf{j}_t^T K) \\ \frac{\partial C}{\partial \mathbf{q}^T} & 0 \end{bmatrix} \begin{bmatrix} \ddot{\mathbf{q}} \\ f_n \end{bmatrix} = \begin{bmatrix} \boldsymbol{\tau} - \mathbf{h}(\mathbf{q}, \dot{\mathbf{q}}) - \mathbf{g}(\mathbf{q}) - \mathbf{D}\dot{\mathbf{q}} \\ \dot{\mathbf{q}}^T \left\{ \frac{\partial}{\partial \mathbf{q}} \left(\frac{\partial C}{\partial \mathbf{q}^T} \right) \right\} \dot{\mathbf{q}} \end{bmatrix}. \quad (6)$$

Because the size of matrix $M(\mathbf{q})$ is generally very large, compelling a large amount of computation to calculate each element of $M(\mathbf{q})$ by using Lagrange method. In our research, we have 10 links, so $M(\mathbf{q})$ is a 10×10 matrix. This implies that analytical deriving of Eq.(4) is

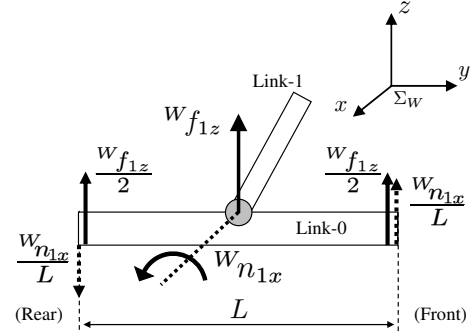


Fig. 4. Transition from (I) to (II) and from (III) to (IV)

almost impossible by hand writing calculation. A ‘‘Newton-Euler’’ method introduced in [17] can calculate such kinds of dynamical coefficients numerically and recursively through forward dynamics calculation. So we use this method in our simulation.

B. Walking Style Representation

The walking sequence of the flat-foot is more complicated than those of the point-foot and the round-foot, because each flat-foot has three contact cases: heel-contact, toe contact and foot contact. As shown in Fig. 3, there are several walking styles (I), (II), \dots (V) in the walking sequence. A walking process may not include all these styles, moving from which one to which phase of the motion depends on the equation of motion and some predefined conditions i.e. shape of the ground, size of foot and so on. All dynamical parameters can affect the resulted motion of walking gait's variety.

Let the forward leg be expressed by ‘‘FL’’ and the backward leg be expressed by ‘‘BL’’, we can describe the characteristics of each walking style as follows.

Style I: Surface-contacting (BL)

Link-0 is surface-contacting without slipping, being regarded as a part of ground.

Style II: Point-contacting (BL)

Link-0 is point-contacting, but constraint condition about Link-0 need not to be incorporated like Eq.(4), that is, the second and third terms should be eliminated, since the motion of Link-0 can be added to the equation of motion as additional state q_0 , setting the number of states of Eq.(6) increase by one.

Style III: Surface-contacting (BL) and point-contacting (FL)

The heel of FL (tip of Link-6) is point-contacting, and BL is surface-contacting which is the same with (I). The constraint condition is required for the heel of FL.

Style IV: Point-contacting for both (BL) and (FL)

The heel of FL (tip of Link-6) is point-contacting, and Link-0 is rotating which is the same with (II). The constraint condition is required for the heel of FL and angle of Link-0 should be considered. In this case, the left-hand side of Eq.(4) is identical to the one of Style II.

Style V: Point-contacting (BL) and surface-contacting (FL)

In this walking style, FL becomes surface-contacting, being regarded as a part of ground. BL is point-contacting under constraint condition. The backward leg can be used for exerting torque by ankle.

C. Transition Conditions among Phases

(1): *from (I) to (II) and from (III) to (IV)*

This change of phase means that the heel of the rear-foot detaches from the ground in Phase (I) or (III). Firstly, reference coordinate of ${}^1\mathbf{f}_1$ (exerting torque to Link-1 whose vector is represented by a coordinates Σ_1 being fixed at Link-1) and ${}^1\mathbf{n}_1$ (exerting torque to Link-1 as the same manner like ${}^1\mathbf{f}_1$) is converted from Σ_1 to Σ_W by ${}^W\mathbf{f}_1 = {}^W\mathbf{R}_1{}^1\mathbf{f}_1$ and ${}^W\mathbf{n}_1 = {}^W\mathbf{R}_1{}^1\mathbf{n}_1$.

Then, projection to z-axis, meaning a vertical axis of the ground of ${}^W\mathbf{f}_1 = [{}^Wf_{1x}, {}^Wf_{1y}, {}^Wf_{1z}]^T$ and projection to x-axis, representing a rotational axis of foot of ${}^W\mathbf{n}_1 = [{}^Wn_{1x}, {}^Wn_{1y}, {}^Wn_{1z}]^T$ are derived by using unit vector $\mathbf{e}_x = [1, 0, 0]^T$ and $\mathbf{e}_z = [0, 0, 1]^T$, as

$${}^Wf_{1z} = \mathbf{e}_z^T {}^W\mathbf{f}_1 \quad (7)$$

$${}^Wn_{1x} = \mathbf{e}_x^T {}^W\mathbf{n}_1 \quad (8)$$

Given that the foot contacts with the ground at two representative points of heel and tiptoe, ${}^Wf_{1z}$ and ${}^Wn_{1x}$ are dispersed and act on both ends of Link-0 as shown Fig. 4.

Here, when resultant forces that act on rear/front of Link-0 are defined as F_R and F_F respectively, we can get two equations below.

$$F_R = \frac{{}^Wf_{1z}}{2} + \frac{{}^Wn_{1x}}{L} \quad (9)$$

$$F_F = \frac{{}^Wf_{1z}}{2} - \frac{{}^Wn_{1x}}{L} \quad (10)$$

Thus, when the value of F_R becomes negative, Link-0 begins to rotate around the tiptoe, which means the heel detaches from the ground. For this reason, inequality shown as Eq. (11) is condition expression for switching.

$$F_L < 0 \quad (11)$$

(2): *from (I) to (III) or from (II) to (IV)*

When the heel of forefoot attaches the ground, the phase is switched from (I) to (III) or from (II) to (IV). Therefore, given z axis of the forefoot's heel is defined as z_6 , switching condition is shown as follows.

$$z_6 \leq 0 \quad (12)$$

(3): *from (III) to (V) or from (IV) to (V)*

When Link-6, defined as a lifting foot's link, becomes surface-contacting, the phase is switched from (III) to (V) or from (IV) to (V). That is, when $q_e (= q_0 + q_1 + \dots + q_6)$ is defined as angle between Link-6 and the ground shown in Fig. 3, switching condition is:

$$q_e \leq 0 \quad (13)$$

TABLE I
PHYSICAL PARAMETERS VALUES IN SIMULATIONS

Link Number	0	1	2	3	4
Mass m_i [kg]	1.0	1.0	1.0	1.5	1.0
Length l_i [m]	0.5	2.0	2.0	1.5	2.0
Radius r_i [m]	(0.8, 0.5)	0.2	0.2	0.2	0.2

Link Number	5	6	7	8
Mass m_i [kg]	1.0	1.0	3.0	1.0
Length l_i [m]	2.0	0.5	2.0	0.5
Radius r_i [m]	0.2	(0.5, 0.8)	0.2	0.5

(4): *from (V) to (I)*

When a condition that tiptoe (the tip of Link-6', which is renamed into Link-6' for the name of Link-6 in phase of (III) or (IV) since the robot's basic configuration of (V) and (I) are identical but the link's numbers are vice versa derived from left leg and right leg being reversed) detaches from the ground is satisfied, phase (V) is switched to phase (I). In this posture, constraint force f_n acts on Link-6'. That is, if the value of f_n is positive, Link-6' contacts with the ground. Meanwhile, if the value of f_n is negative, Link-6' starts lifting, then the condition is:

$$f_n < 0 \quad (14)$$

IV. SIMULATION RESULTS

We perform simulations to verify the effectiveness of the proposed visual lifting bipedal walking method. Graphic presentation of robot's walking gait transition is conducted by "Open GL", and the robot's parameter values used in the following analyse are shown in Table 1. Here, to evaluate the "visual lifting" ability in bipedal walking performance, we assume the visual measurement is correct, including no error. That is, the values of ${}^E\mathbf{T}_M(\hat{\psi}(t))$ in Eq. (1) is calculated based on the camera position given by the robot kinematics, with the object position in Σ_W given in advance.

A. Walking Simulations under Different Gaits

In this simulation, we compared the walking performance under the same physical parameters (see Table 1) and the same initial conditions (the bipedal robot's initial posture and the given torque on the waist to drive the leg to take a step forward), but different visual feedback gains (\mathbf{k}_v in Eq. (2)).

Firstly, we set $\mathbf{k}_v = (150, 150, 150)$. Figure. 5 is the head trajectory of y-coordinate (walking direction) and z-coordinate (upright direction) values that are normalized by body height. Figure. 5 (a) shows that the robot is walking forward with a distance of 0.6 (body height) in 10[s], (b) shows that the head height is decreasing during walking from 1 to 0.85 (body height), and the height has been retained during walking. Figure. 6 (a) shows how walking style changes in this situation. It is a rhythmic motion that

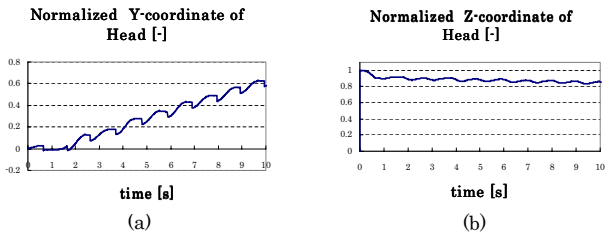


Fig. 5. Head trajectory of y-coordinate and z-coordinate in the case of $k_v = (150, 150, 150)$. Both y-coordinate and z-coordinate values are normalized by body height.

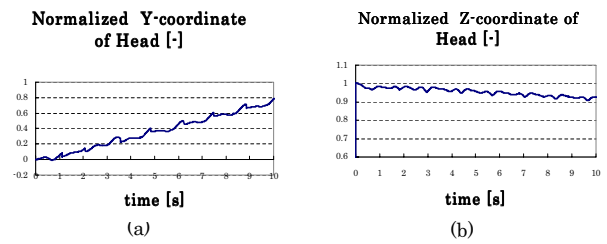


Fig. 8. Head trajectory of y-coordinate and z-coordinate in the case of $k_v = (900, 900, 900)$. Both y-coordinate and z-coordinate values are normalized by body height.

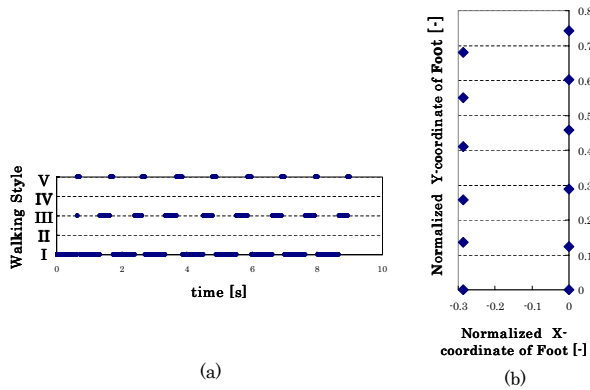


Fig. 6. (a) Step changing with respect to time. (b) Foot trajectory on the ground. This simulation is in the case of $k_v = (150, 150, 150)$. Both x-coordinate and y-coordinate values are normalized by body height. From (b) we can calculate the average length of one walking step is about 0.145 normalized by body height.

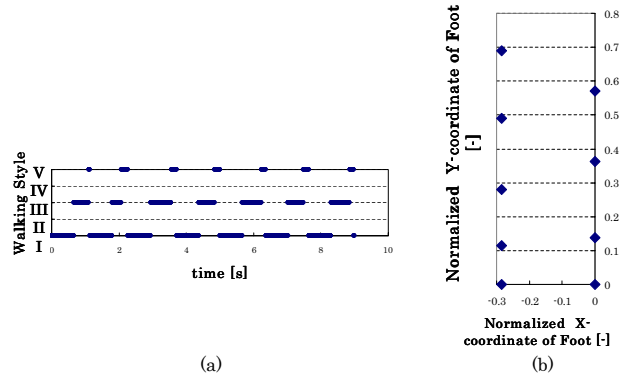


Fig. 9. (a) Step changing with respect to time. (b) Foot trajectory on the ground. This simulation is in the case of $k_v = (900, 900, 900)$. Both x-coordinate and y-coordinate values are normalized by body height. From (b) we can calculate the average length of one walking step is about 0.19 normalized by body height.

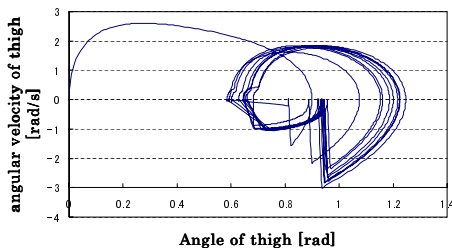


Fig. 7. Leg trajectory of the dynamic walking, expressed by phase portrait, in the case of $k_v = (150, 150, 150)$.

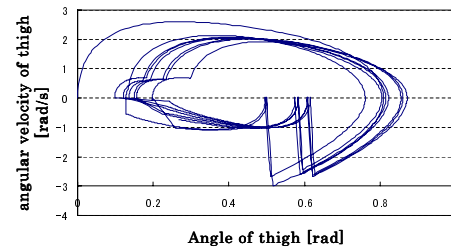


Fig. 10. Leg trajectory of the dynamic walking, expressed by phase portrait, in the case of $k_v = (900, 900, 900)$.

each one is changing by Style I \rightarrow Style III \rightarrow Style V with a period of 0.9[s]. Figure. 6 (b) is foot trajectory on the ground. We can calculate the average length of one walking step is about 0.145 body height. Figure. 7 shows the leg trajectory expressed by phase portrait: the relation of thigh angle (the angle between two legs) and its velocity. Since the initial posture is thigh angle is 0[rad], the single line from 0[rad] to 0.9[rad] represents the first step of the walking that performed by one leg, then the other leg follows but does not move over the first one, so the thigh angle decreased to about 0.6[rad]. Then another walking cycle starts, first step is from 0.6[rad] to 1.2[rad], second step from 1.2[rad] return to about 0.6[rad], the following gaits appeared in the same manner.

To compare with the above simulation, now we set $k_v = (900, 900, 900)$, all other initial conditions are kept to be the same values. Figure. 8 to Fig. 10 are the simulation results in this situation. Comparing Fig. 5 with Fig. 8, we can see that the robot is walking forward faster, with a walked distance of 0.8 (body height) at 10[s], but the head height is only decreased 0.08(body height), smaller than the above simulation which is 0.15(body height) depicted in Fig. 5(b). Figure. 9 shows the walking is also a rhythmic motion that composed by Style I \rightarrow Style III \rightarrow Style V, the period is about 1.1[s]. From Fig. 6 (b), we get the average length of one walking step is about 0.19 body height, which is longer than the above one. Leg trajectory expressed in Fig. 10 shows the walking to be stable. The animation of robot's gait during this simulation of Visual Lifting Bipedal Walking in the way

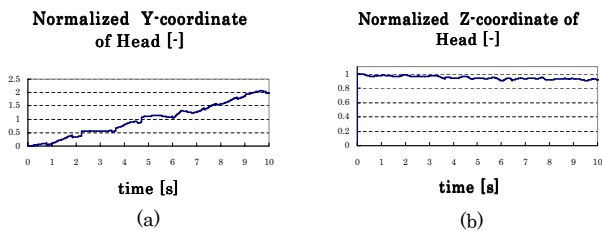


Fig. 12. Head trajectory of y-coordinate and z-coordinate in the case of all walking styles included. Both y-coordinate and z-coordinate values are normalized by body height.

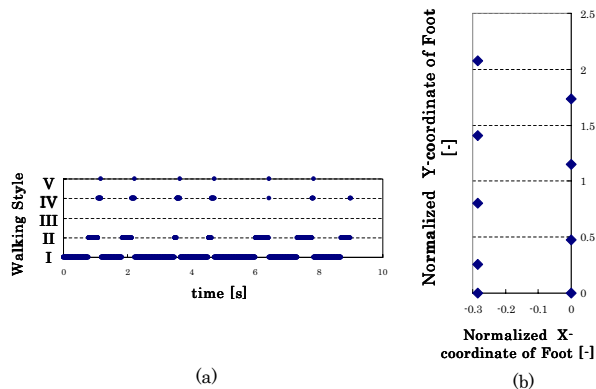


Fig. 13. Leg trajectory of the dynamic walking, expressed by phase portrait.

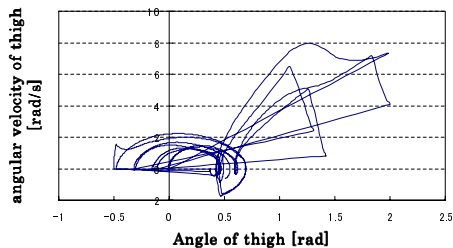


Fig. 14. Head trajectory of y-coordinate and z-coordinate in the case of all walking styles included. Both y-coordinate and z-coordinate values are normalized by body height.

of Style I \rightarrow Style III \rightarrow Style V ($k_v = (900, 900, 900)$) is depicted in Fig. 11.

By comparing this two simulations, we can give the conclusion that under the same initial conditions, high visual feedback gain values lead to more effective “visual lifting” ability, with smaller head height decline and longer walking step.

B. Comparison of Different Walking Styles

In this simulation, we compared the walking performance of different walking styles. We keep the same physical parameters (see Table 1), but change the initial conditions. The bipedal robot’s initial posture is the same with the above simulations whose results are shown in Figs.5 to 11, but in this section the given torque on the waist to drive the leg to take a step forward is changed. Thus the resulted walking style is changed as Style I \rightarrow Style II \rightarrow Style IV \rightarrow

Style V, which is more similar with the walking motion of human beings, with much longer walking step.

Figure. 12 to Fig. 14 are the simulation results in this situation. Compared with Fig. 8, Fig. 12 shows that the robot is walking forward much faster, with a distance of 2 (body height) in 10[s], the head height is decreased by only 0.1(body height). Figure. 13 shows the walking is a rhythmic motion that composed by Style I \rightarrow Style II \rightarrow Style IV \rightarrow Style V, but the period is varying, and the duration time of Style I and Style II is different, which indicates that the motion has not fallen in limit cycle. This also be observed in Fig. 14. The changing of the angle between two legs is almost in the same way in the above two simulations, but in this case the trajectory is not much overlap each other, which means the walking motion is less stable than the previous simulations.

So we can say that “Style I \rightarrow Style II \rightarrow Style IV \rightarrow Style V” walking is very effective, it can walk forward 2 (body height) in 10[s]. However, the simulation shows that this walking way is not stable, from a view point of the phase portrait does not tend to converge into stable limit cycle, thus leaving a room to discuss how to make this walking dynamics more stable.

V. CONCLUSION

In this paper, we proposed a “Visual Lifting Bipedal Walking” strategy, by using the visually measured information to control the robot for keeping a desired head-top’s position/orientation to avoid falling down.

Simulations has been performed to present the effectiveness of “visual lifting” ability with comparing two simulations under different visual feedback gain, the results show that high visual feedback gain values lead to more effective “visual lifting” ability, with smaller head height decline and longer walking step.

Also, by changing the initial conditions, we confirmed that two gait patterns appeared, i.e., “Style I \rightarrow Style III \rightarrow Style V” and “Style I \rightarrow Style II \rightarrow Style IV \rightarrow Style V”. The second walking gait pattern is more effective with longer walking distance acheived, but this walking way is not stable, since the phase portrait does not tend to converge into stable limit cycle. In the future work, we will deal with this unstable problem, try to make the robot perform an effective and stable walking by “visual lifting”.

REFERENCES

- [1] D. Djoudi, C. Chevallereau, and J. Grizzle, *A path-following approach to stable bipedal walking and zero moment point regulation*, in Proc. IEEE Int. Conf. Robot. Autom., Rome, Italy, 2007, pp. 3597-3602.
- [2] C. Chevallereau, D. Djoudi, and J. Grizzle, *Stable bipedal walking with foot rotation through direct regulation of the zero moment point*, IEEE Trans. Robot., vol. 25, no. 2, pp. 390-401, Apr. 2008
- [3] J. Yamaguchi, S. Inoue, D. Nishino, and A. Takanishi, *Development of a bipedal humanoid robot having antagonistic driven joints and three dof trunk*, in Proc. of the 1998 IEEE/RSJ Int. Conf. on Intelligent Robots and Systems, pp. 96101, 1998.
- [4] K. Nagasaka, M. Inaba, and H. Inoue, *Walking pattern generation for a humanoid robot based on optimal gradient method*, in proceeding of IEEE Int. Conf. on Systems, Man, and Cybernetics, 1999.

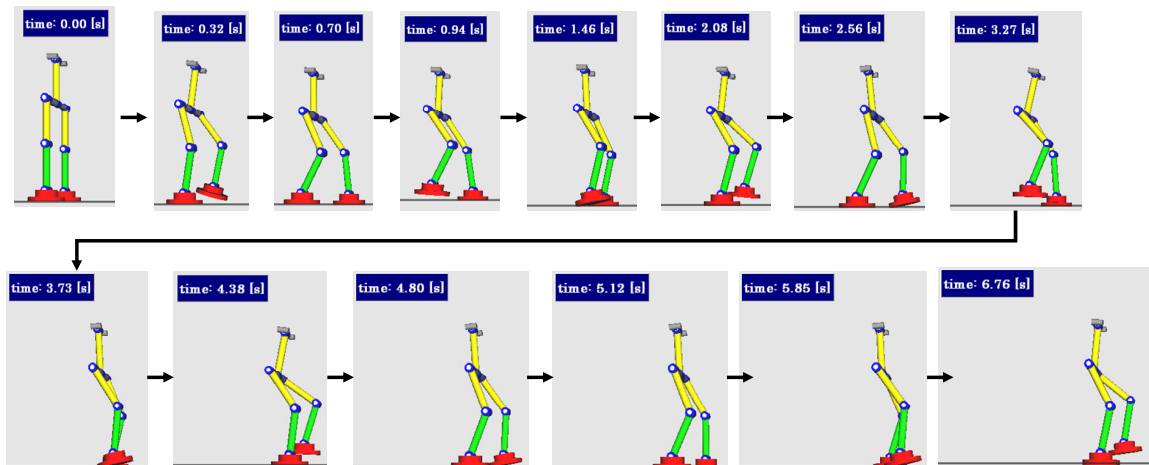


Fig. 11. Visual Lifting Bipedal Walking, Style I \rightarrow Style III \rightarrow Style V. ($k_v = (900, 900, 900)$).

- [5] Qiang Huang and Yoshihiko Nakamura, *Sensory Reflex Control for Humanoid Walking*, IEEE Trans. Robot., vol. 21, no. 5, pp. 977-984, Oct. 2005.
- [6] K. Nishiwaki and S. Kagami, *Online walking control system for humanoids with short cycle pattern generation*, The International Journal of Robotics Research, vol. 28, no. 6, pp. 729-742, 2009.]
- [7] Koichi Nishiwaki and Satoshi Kagami, *Online Design of Torso Height Trajectories for Walking Patterns that takes Future Kinematic Limits into Consideration*, IEEE Int. Conf. on Robotics and Automation, pp. 2029-2034, 2011].
- [8] Wei Song and Mamoru Minami, *Hand & Eye-Vergence Dual Visual Servoing to Enhance Observability and Stability*, IEEE Int. Conf. on Robotics and Automation (ICRA), pp.714-721, 2009.
- [9] Wei Song and Mamoru Minami, *Stability / Precision Improvement of 6-DoF Visual Servoing by Motion Feedforward Compensation and Experimental Evaluation*, IEEE Int. Conf. on Robotics and Automation (ICRA), pp.722-729, 2009.
- [10] Wei Song, Mamoru Minami, Fujia Yu, Yanan Zhang and Akira Yanou, *3-D Hand & Eye-Vergence Approaching Visual Servoing with Lyapunov-Stable Pose Tracking*, IEEE Int. Conf. on Robotics and Automation (ICRA), pp.5210-5217, 2011.
- [11] Fujia Yu, Wei Song and Mamoru Minami, *Visual Servoing with Quick Eye-Vergence to Enhance Trackability and Stability*, IEEE International Conference on Robotics and Automation (IROS), pp.6228-6233, 2009.
- [12] E. Mails, *Improving vision-based control using efficient second-order minimization techniques* in Proceedings of IEEE International Conference on Robotics and Automation, pp. 1843-1848, 2004.
- [13] Wolfgang Sepp, Stefan Fuchs and Gerd Hirzinger, *Hierarchical Featureless Tracking for Position-Based 6-DoF Visual Servoing*, Proceedings of the 2006 IEEE/RSJ Int. Conf. on Intelligent Robotics and Systems (IROS), pp.4310-4315, 2006.
- [14] C. Dune, E. Marchand, C. leroux, *One Click Focus with Eye-in hand/ Eye-to hand Cooperation*, IEEE Int. Conf. on Robotics and Automation (ICRA), pp.2471-2476, 2007.
- [15] Alexander Andreopoulos, Stephan Hasler, Heiko Wersing, Herbert Janssen, John K. Tsotsos, and Edgar Kirner, *Active 3D Object Localization Using a Humanoid Robot*, IEEE Trans. Robot., vol. 27, no. 1, pp. 47-64, Feb. 2011.
- [16] Tsuneo Yoshikawa, *Foundations of Robotics*, MIT Press, 1990.
- [17] Tsutomu Mita, Koichi Osuka, *Introduction to Robot Control*, ISBN 4-339-03137-2, 1989.